bioRxiv preprint doi: https://doi.org/10.1101/2020.03.17.996124; this version posted March 18, 2020. The copyright holder for this preprint (which was not certified by peer review) is the author/funder. All rights reserved. No reuse allowed without permission.

Structure of population activity in primary motor cortex for single finger flexion and extension

Spencer A. Arbuckle[1a], Jeff Weiler[1a], Eric A. Kirk[1b], Charles L. Rice[1b], Marc Schieber[2c], J. Andrew Pruszynski[1a,d,e], Naveed Ejaz[1a], Jörn Diedrichsen[1a,f]

1. Western University, London, Ontario, Canada
2. The Del Monte Institute for Neuroscience, University of Rochester, Rochester, New York, USA

a. Brain and Mind Institute
b. School of Kinesiology, Faculty of Health Sciences, Department of Anatomy and Cell Biology, Schulich School of Medicine & Dentistry
c. Departments of Neuroscience, Neurology, Biomedical Engineering, & Center for Visual Science
d. Departments of Physiology and Pharmacology, & Psychology
e. Robarts Research Institute
f. Departments of Statistical and Actuarial Sciences, & Computer Science

Correspondence
Jörn Diedrichsen, Brain and Mind Institute, University of Western Ontario, London, Canada. jdiedric@uwo.ca.

Acknowledgements
The work was supported by Canada First Research Excellence Fund (BrainsCAN) collaborative postdoctoral grant awarded to NE, JW, and SA, and a Discovery Grant from the Natural Sciences and Engineering Research Council (NSERC, RGPIN-2016-04890) to JD. Functional imaging costs were partly supported by a Platform Support Grant from Brain Canada and BrainsCAN. SA and EK are supported by doctoral scholarships from NSERC (PGSD3-519263-2018 and CGSD3-519372-2018, respectively). JW is supported by a BrainsCAN Postdoctoral Fellowship. MHS was supported by NINDS grants NS27686 and NS102343. JP is supported by the Canada Research Chairs program. We thank Marcus Saikaley for help with human EMG data collection.

Author contributions
SA, NE, & JD designed the experiment; SA collected and analyzed the fMRI data; JW, EK, CR, NE, & SA collected the EMG data; SA, NE, & JW analyzed the EMG data; MS collected the spiking data; SA processed and analyzed the spiking data; SA prepared figures; SA, AP, & JD wrote the manuscript.

Conflict of interest
The authors declare no conflict of interest.

bioRxiv preprint doi: https://doi.org/10.1101/2020.03.17.996124; this version posted March 18, 2020. The copyright holder for this preprint (which was not certified by peer review) is the author/funder. All rights reserved. No reuse allowed without permission.

Abstract

How is the primary motor cortex (M1) organized to control fine finger movements? We investigated the population activity in M1 for single finger flexion and extension, using 7T functional magnetic resonance imaging (fMRI) in human participants, and compared these results to the neural spiking patterns recorded in monkeys performing the identical task. fMRI activity patterns were distinct for movements of different fingers, but quite similar for flexion and extension of the same finger. In contrast, spiking patterns in monkeys were quite distinct for both fingers and directions, similar to what was found for muscle activity patterns in humans. Given that fMRI reflects predominantly input and recurrent activity, these results suggest an architecture in which neural populations that control flexion or extension of the same finger receive similar inputs and interact tightly with each other, but produce distinct outputs.

bioRxiv preprint doi: https://doi.org/10.1101/2020.03.17.996124; this version posted March 18, 2020. The copyright holder for this preprint (which was not certified by peer review) is the author/funder. All rights reserved. No reuse allowed without permission.

Introduction

Dexterous movements of fingers require accurate coordination of different hand muscles. Hand muscles are innervated by motorneurons in the ventral horn of the spinal cord, which receive direct and indirect projections from the hand region of the contralateral primary motor cortex (M1) (Lemon, 2008). In monkey species that are able to better individuate their fingers, direct (monosynaptic) projections from M1 to ventral horn motor neurons are more pronounced (Heffner & Masterton, 1983; Bortoff & Strick, 1993). Lesions to the corticospinal tract (Tower, 1940; Lawrence & Kuypers, 1968; Lawrence & Hopkins, 1976; Sasaki et al., 2004) or to M1 (permanent: Liu & Rouiller, 1999; Darling et al., 2009; reversible: Schieber & Poliakov, 1998) result in a significant loss of finger individuation. Such symptoms are also reported in human stroke patients who have damage to the hand area of M1 or the descending corticospinal pathway (Lang & Schieber, 2003; Xu et al., 2017). These results indicate that M1 is important for the fine control of individuated finger movements.

What is less well understood is how this cortical control module for finger movements is organized. Here, we studied this question by investigating cortical activation patterns evoked during flexion and extension of individual fingers. Previous results in monkeys (Schieber & Hibbard, 1993; Schieber & Poliakov, 1998) have indicated that motor cortical neurons have complex tuning functions, often responding to movements of multiple fingers and to both flexion and extension movements. Therefore, there exists no clearly organized “map”, with separate regions dedicated to the control of a single finger. Thus, the structure of population activity in M1 must be organized by some other principle.

One plausible principle is that the statistics of natural human hand use shapes the organization of neuronal populations in the hand region of M1. This idea predicts that movements that commonly co-occur in every-day life are represented in overlapping substrates in M1 (Graziano & Aflalo, 2007). Specifically, fingers with high correlations between their joint-angle velocities during everyday hand movements (Ingram, Körding, Howard, & Wolpert, 2008) have been shown to have more similar M1 activity patterns (Ejaz, Hamada, & Diedrichsen, 2015). The correlation structure of everyday movements nearly fully explained the relative similarities of M1 finger activity patterns, and fit the data better than a model that used the similarity of the required muscle activity patterns (i.e. predicting that movements that use similar muscles also should have similar activity patterns) or a somatotopic model (i.e. predicting that fingers are represented in an orderly finger map).

bioRxiv preprint doi: https://doi.org/10.1101/2020.03.17.996124; this version posted March 18, 2020. The copyright holder for this preprint (which was not certified by peer review) is the author/funder. All rights reserved. No reuse allowed without permission.

In this paper, we asked to what degree do these findings generalize to flexion and extension movements of the fingers. We measured the activity evoked in the hand area of M1 using high-field functional magnetic resonance imaging (fMRI) while human participants performed near-isometric single finger flexion and extension presses with their right hand. By extrapolating the model used in Ejaz et al. (2015) to this situation, we predicted that each movement should have its own, clearly separated representation in M1, as flexion and extension can never co-occur. Indeed, it has been recently suggested that the motor cortex has multiple representations of each finger, one dedicated to flexion and one to extension (Huber et al., 2020).

We found, however, that the measured fMRI patterns for flexion and extension of the same finger were strikingly similar, much more similar than would be expected for two movements that cannot co-occur. To understand these results better, we re-investigated the representational structure of single-neuron activity in M1 of two macaque monkeys trained on the same flexion-extension task (data from Schieber & Rivlis, 2005; Schieber & Rivlis, 2007). The spiking patterns in monkeys were quite distinct for fingers and directions. Together, these results suggest a specific organization of finger movement representations in the primary motor cortex.

Results

M1 fMRI activity patterns differ strongly for different fingers, not for direction.

We measured activity patterns evoked in M1 in human participants (n=9) while they performed a near-isometric finger flexion-extension task in a 7T MRI scanner. Participants' right hands were clamped in a device that had force transducers mounted both above (extension) and below (flexion) each finger (Fig. 1A) to record forces produced at the distal phalanges. The device limited the overall degree of movement to a few millimeters, thereby making the task near-isometric. On each trial, participants were cued to press a single finger in one direction, while keeping the other fingers as relaxed as possible (Fig. 1B). They had to reach the required force level, hold it for 1 second, and then simply relax their hand to let the force passively return to baseline. This aspect of the task instruction was critical to ensure that participants did not activate the antagonist muscles during release.

Figure 1C shows the activity patterns measured in left M1 (contralateral to movement) for one participant during right-handed finger presses at 2N. As previously observed (Ejaz et al., 2015), the activity patterns did not consist of focal regions of activity dedicated to each finger. Rather, the spatial patterns were complex and involved multiple

bioRxiv preprint doi: https://doi.org/10.1101/2020.03.17.996124; this version posted March 18, 2020. The copyright holder for this preprint (which was not certified by peer review) is the author/funder. All rights reserved. No reuse allowed without permission.

overlapping regions within the M1 hand area. Furthermore, the inter-subject variability in the spatial organization of these patterns was considerable (see supp. fig. S1).

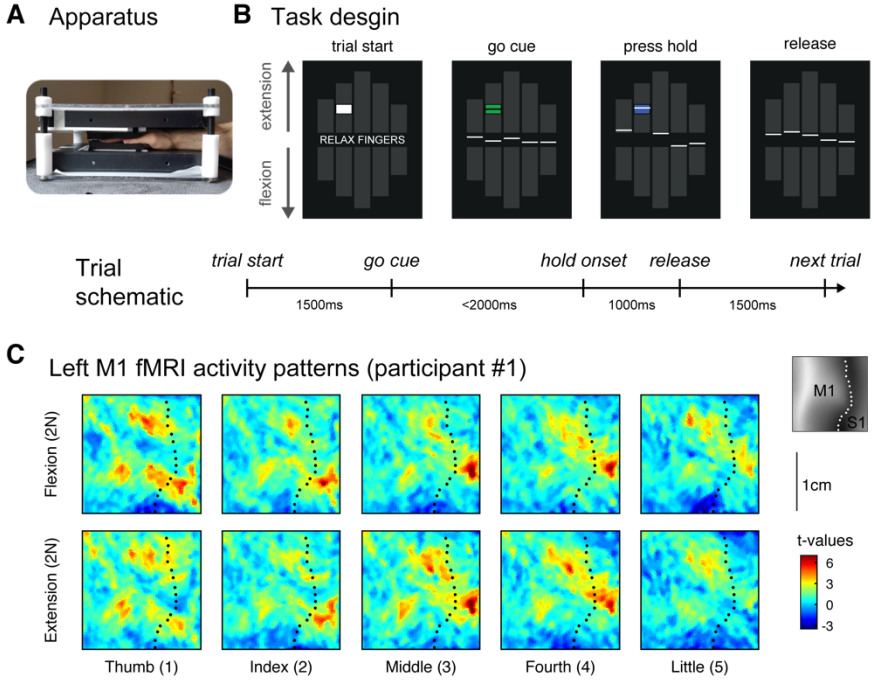

Figure 1 | **Measuring activity patterns for finger flexion and extension in human M1.** (**A**) Human participants made isometric single finger presses in the flexion and extension directions on a custom-built keyboard. Each finger of the right hand was clamped between two keys, and each key was associated with a force transducer either above (keyboard on top of hand) or below (keyboard under the hand) the key to monitor forces applied in the flexion and extension directions, respectively. (**B**) Visual feedback display shown to the participant. The white lines represent the produced force for each finger. Applying flexion to a finger key moved the associated line down (vice-versa for extension). The cue box (centred at target force) was initially presented as white at the trial start, and turned green to cue the participant to make the finger press (here, index finger extension). The box turned blue to instruct participants to maintain the current force. At the end of the press hold, the cue box disappeared and participants relaxed their hand. The associated timing of these events are included in the trial schematic. (**C**) Evoked fMRI activity maps (t-values) for participant #1 for each of the 5 fingers pressing in the extension and flexion directions at 2N. Maps are shown in the hand-knob region of the left (contralateral) hemisphere. The black dotted line shows the fundus of the central sulcus. For two additional participants, see supplementary figure S1. Average finger enslaving is shown in supplementary figure S2 (enslaving in the flexion direction are positive values, vice versa).

One common observation across all participants, however, was that the activity patterns were different between different fingers (e.g. index flexion vs. fourth flexion), but rather similar for flexion and extension of the same finger (e.g. index flexion vs. index extension). To quantify these observations, we calculated a measure of dissimilarity (crossnobis distance, see Methods) between each pair of fMRI patterns. Large dissimilarity values indicate that the two patterns are quite distinct with little overlap. A value of zero indicates that the two patterns are identical, and the measured patterns

bioRxiv preprint doi: https://doi.org/10.1101/2020.03.17.996124; this version posted March 18, 2020. The copyright holder for this preprint (which was not certified by peer review) is the author/funder. All rights reserved. No reuse allowed without permission.

only differ by noise. We restricted the analysis to conditions with matched force levels across flexion and extension. The group-averaged representational dissimilarity matrix (RDM) is shown in figure 2A. Both within the finger flexion and extension conditions, there was a characteristic structure with the thumb activity pattern being the most distinct and neighbouring fingers tending to have more similar activity patterns. Across directions, activity patterns evoked by pressing the same finger in different directions were the most similar. This representational structure was quite stable across participants (average inter-participant Pearson's r=0.790, 95% CI: [0.754-0.820]).

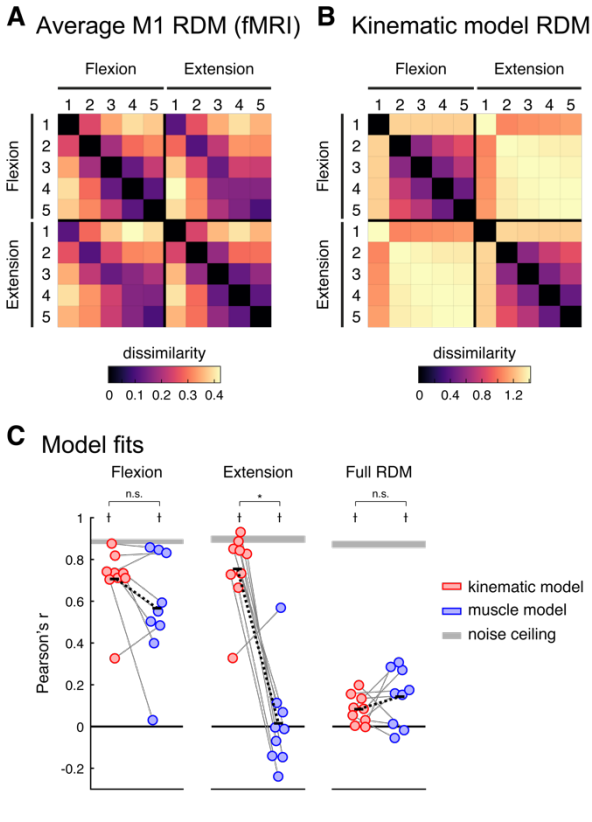

Figure 2 | Representational structure of fingers and direction in human M1. (**A**) Group average of the fMRI representational dissimilarity matrix (RDM). (**B**) Predicted RDM from the kinematic model. To aid visual inspection, the values of the RDMs in **A** and **B** are plotted as the square-root of the dissimilarities. All statistical analyses of the RDMs are done on squared distances. (**C**) Model fits (Pearson's correlation) of the kinematic (red) and muscle models to the M1 RDM for flexion, extension, and the full RDMs. The muscle model was specific to each participant and was estimated from the EMG data. The grey bars denote noise ceilings (theoretically the best possible fits). Each dot reflects one participant, and thin grey lines connect fits of each model to the same participant. Black bars denote the means, and black dashed lines denoted the mean paired difference. *significant differences between model fits (one-sided paired t-test, $p<0.05$); ǂsignificantly lower than the noise ceiling (two-sided paired t-test, $p<0.05$); n.s. not significant ($p>0.05$).

To obtain predictions for flexion and extension movements, we needed to adapt the natural usage model, proposed by Ejaz et al. (2015). This model used kinematic finger data, specifically the joint-angle velocities of the metacarpal (MCP) joints, recorded while subjects participated in their normal, every-day tasks (data from Ingram et al., 2008). Fingers were predicted to have more similar representations if their movement velocities, across flexion and extension, were positively correlated. For the current experiment, we split the data into periods of finger flexion and finger extension (see methods), resulting in 10 time series, and calculated the correlation between them (after taking the absolute value).

bioRxiv preprint doi: https://doi.org/10.1101/2020.03.17.996124; this version posted March 18, 2020. The copyright holder for this preprint (which was not certified by peer review) is the author/funder. All rights reserved. No reuse allowed without permission.

The estimated kinematic RDM (Fig. 2B) showed similar structures within flexion and extension movements. The thumb was the most distinct compared to the other fingers, and for the remaining fingers there was a clear similarity structure with neighbouring fingers more similar than non-neighbouring. This structure very closely mirrored those found for fMRI activity patterns: flexion and extension fMRI RDMs correlated strongly with the corresponding kinematic models for flexion (r=0.727 [0.635-0.800]) and extension (r=0.797 [0.684-0.873]) RDMs (Fig. 2C, red). Compared to the noise ceiling (grey bar in Fig 2C, which reflects the best possible model fit given measurement noise: see methods) the natural use model accounted for 79.9% and 84.9% of the variance in the flexion and extension RDMs, respectively.

In contrast, the kinematic model completely failed to predict the relationships between activity patterns for flexion and extension. Because flexion and extension of the same finger can never co-occur, the kinematic model predicts that the movements are associated with quite distinct cortical activity patterns. The measured fMRI patterns, however, were rather similar for these two actions. As a result, the full kinematic model was not a good fit to the full fMRI RDM (r=0.086 [0.038-0.133]), much below the noise ceiling (r=0.875 [0.822-0.913]).

Thus, although the statistics of movement co-occurrence was a good predictor for representational similarity between the activity patterns for different fingers (i.e. within flexion or extension), this simple model failed to predict the relative organization of the patterns for flexion and extension of the same finger. Even though flexion and extension of the same finger cannot co-occur, their fMRI activity patterns were highly similar. In the remainder of the paper, we explore a number of possible explanations for this finding and propose a candidate model of the organization.

Similarities of cortical representations for presses in different directions cannot be explained by the patterns of muscle activity.

We first considered the possibility that the structure of similarity between flexion and extension presses can be explained by the patterns of muscle activity required by these movements. Specifically, it is possible that participants co-contracted both agonist and antagonist muscles, or that they activated the antagonistic muscles when returning to baseline. Given the temporally sluggish nature of the blood-oxygen level-dependent (BOLD) signal measured with fMRI, either behaviour could cause the cortical activity patterns evoked during flexion to resemble activity patterns during extension (and vice versa). Therefore, we conducted a control experiment with the same participants outside the MR scanner, during which we recorded surface electromyography (EMG) from 14

bioRxiv preprint doi: https://doi.org/10.1101/2020.03.17.996124; this version posted March 18, 2020. The copyright holder for this preprint (which was not certified by peer review) is the author/funder. All rights reserved. No reuse allowed without permission.

sites of the hand and forearm in the participants (Fig. 3A), while they performed the same isometric finger flexion-extension task as in the fMRI session. Performance on the task was comparable to that during the fMRI scan.

As an example, the participant-averaged EMG data from an electrode placed above the abductor digiti minimi (ADM) muscle (Fig. 3B) showed that the ADM muscle was recruited only during the flexion of the little finger. During extension of the same finger, the muscle was silent, both during hold and release. In general, we found very little evidence for co-contraction of the antagonist muscle.

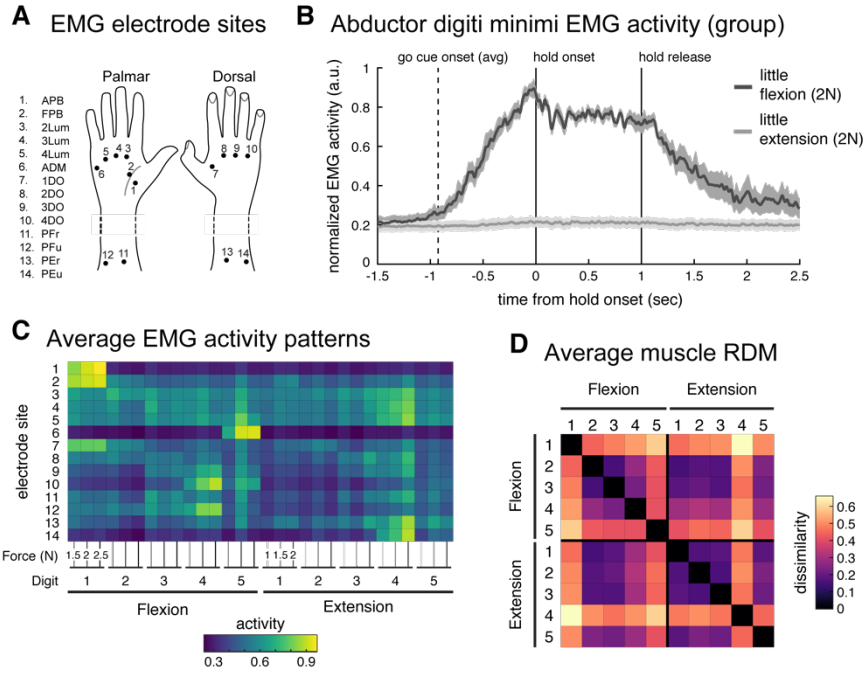

Figure 3 | Quantifying similarity of muscle activity patterns during finger flexion and extension. (**A**) Fourteen surface electrode sites. (**B**) Group averaged EMG (normalized to peak activity from this electrode) from the abductor digiti minimi (ADM) muscle during 2N little finger flexion (dark grey) and extension (light grey) trials, aligned to hold onset (0s). During extension movement (light grey trace, >1000ms), this flexor muscle was not recruited. Shaded areas reflect standard error of the mean. Traces were smoothed with a gaussian kernel (FWHM=25ms). (**C**) Average muscle activity across participants, normalized by peak activation across conditions (per participant), recorded from the 14 electrode sites during the flexion extension task. Each condition was measured under 3 force conditions. (**D**) Group average representational dissimilarity matrix (RDM) of the muscle activity patterns. As in figure 2, the RDM is plotted as square-root dissimilarities to aid visual inspection. Average finger enslaving is shown in supplementary figure S3 (enslaving in the flexion direction are positive values, vice versa).

For a quantitative analysis, we averaged the muscle activity from the time of the go-cue to the end of the hold phase. The EMG patterns averaged across participants (Fig. 3C) already allow for two observations. First, the muscle activities for the same movement at different force levels were very similar and increased with increasing force.

bioRxiv preprint doi: https://doi.org/10.1101/2020.03.17.996124; this version posted March 18, 2020. The copyright holder for this preprint (which was not certified by peer review) is the author/funder. All rights reserved. No reuse allowed without permission.

The average correlation across force levels for each finger-direction combination was high, indicating the same muscles were consistently recruited to perform the same finger press across different force levels (within participant correlations: r=0.858 [0.805-0.898]). Second, quite distinct muscle groups were recruited to produce forces with the same finger in different directions. The average correlation between the pattern of muscle activity recruited to press the same finger in different directions was low (within participant correlations: r=0.245 [0.151-0.334]).

We then derived a muscle-based RDM by calculating the crossnobis dissimilarity between normalized activity patterns for each condition. As for the fMRI analysis, we included the patterns for the matched force conditions only. The group averaged matrix RDM (Fig. 3D) was only moderately stable across participants (average inter-participant Pearson's r=0.490 [0.380-0.586]), likely reflecting the fact that there was some degree of inter-individual variation in electrode placement.

We tested to what degree the patterns of muscle activity, specific to each participant, could explain the cortical similarity structure between individual finger movements within the flexion or extension directions. For the flexion direction, the fit of the muscle model (r=0.622 [0.422-0.765]) was lower than that for the kinematic model in 6 out of 9 participants (Fig. 2C), but the difference did not reach statistical significance (one-sided t-test kinematic>muscle: t_8=1.636, p=0.0702). For the extension direction, the muscle model fit substantially worse (r=0.023 [-0.145-0.190]), significantly less than the kinematic model (one-sided t-test kinematic>muscle: t_8=5.531, p=0.0003). These results generally confirm the results reported in Ejaz et al. (2015) and extend them to extension movements.

Critically, however, the muscle activity model did not provide a good explanation for the similarity between flexion and extension patterns. The fit for the full muscle model (r=0.145 [0.056-0.233]) was as poor as for the kinematic model (two-sided t-test muscle vs. kinematic: t_8=1.064, p=0.3186) and significantly below the noise ceiling (two-sided t-test noise ceiling vs. muscle: t_8=12.706, p=1.3849e-6). Thus, neither the co-occurrence of movements, nor the pattern of muscle activities can explain the high similarity of activity patterns for finger flexion and extension in M1.

M1 spiking output differs equally for fingers and direction.

An alternative explanation for this observation is that the overlapping fMRI activity patterns for flexion and extension reflect shared inputs to these cortical areas. The neuronal population that predominantly controls flexion of a finger should receive sensory input from that finger, just as the neural population that controls finger extension.

bioRxiv preprint doi: https://doi.org/10.1101/2020.03.17.996124; this version posted March 18, 2020. The copyright holder for this preprint (which was not certified by peer review) is the author/funder. All rights reserved. No reuse allowed without permission.

Furthermore, these two populations should be closely connected to facilitate tight coordination. Such common input or mutual interaction would be strongly reflected in fMRI measurements because the cortical Blood Oxygen Level Dependent (BOLD) signal reflects excitatory inputs and local synaptic signaling to a much larger degree than the spiking activity of output neurons (Logothetis, Pauls, Augath, Trinath, & Oeltermann, 2001). If this idea is correct, then the flexion and extension spiking patterns of the principal output neurons of M1 should be quite distinct.

To test this prediction, we re-analyzed population spiking activity of M1 neurons during an equivalent single-finger individuation task in two trained non-human primates (*Macaca mulatta*, data from Schieber & Rivlis, 2005 & 2007). Indeed, we had designed the behavioural task for the fMRI to closely matched the task for the non-human primates, such that we could make strong comparisons across species and measurement modalities. Figure 4A shows the condition averaged firing rate traces from a single neuron from this data set. This neuron displayed strong preference (increased firing rates) for flexion of the middle finger and extension of the index finger. As previously reported (Schieber & Hibbard, 1993), most neurons in M1 demonstrated complex tuning across fingers and directions (Fig. 4B and supplementary figure S4).

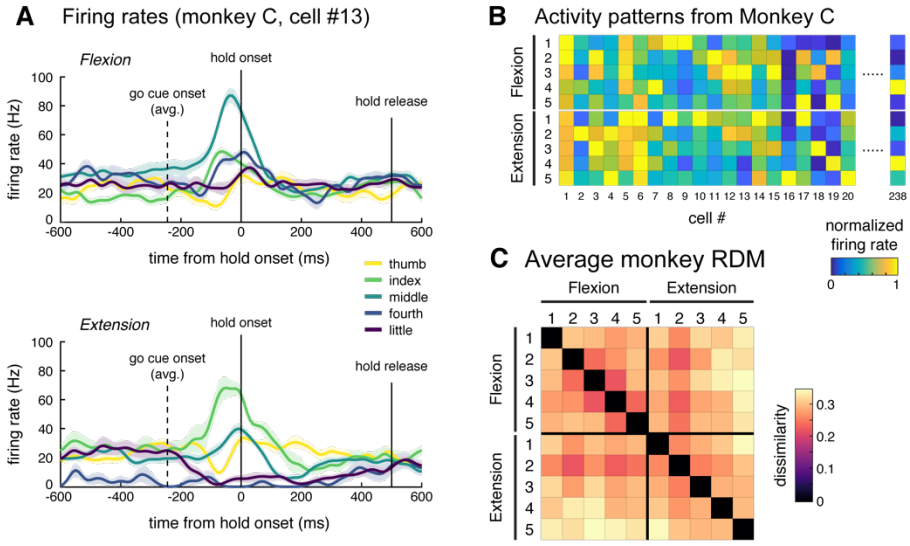

Figure 4 | **Analysis of M1 spiking activity during monkey single finger flexion and extension.** (**A**) Trial averaged firing rates from one cell (monkey C). Traces are aligned to press onset (0s). This cell demonstrates selective tuning to middle finger flexion and index finger extension. Firing rates were calculated for 10ms bins and smoothed with a gaussian kernel (FWHM=50ms). (**B**) Averaged firing rates for a subset of cells from monkey C, arranged by condition. Cell #13 is plotted in **A**. Firing rates are normalized to the peak rate per cell. (**C**) Average monkey RDM (square-root dissimilarities). For spike traces from three additional cells from monkey C see supplementary figure S4.

bioRxiv preprint doi: https://doi.org/10.1101/2020.03.17.996124; this version posted March 18, 2020. The copyright holder for this preprint (which was not certified by peer review) is the author/funder. All rights reserved. No reuse allowed without permission.

To compare the representational structure from spiking data to that obtained with fMRI, we calculated the mean firing rate for each neuron from the go-cue onset to the end of the hold phase during each trial. We then calculated dissimilarities between the population responses for different conditions (see Methods), similar to the analysis of the human EMG and fMRI data. The average RDM is shown in Figure 4C. Similar to the structure of representations in human M1, the thumb activity patterns for both directions were the most distinct, and neighbouring fingers had more similar activity patterns. In contrast to the fMRI data, however, the spiking patterns for flexion and extension of the same finger were quite distinct.

To quantify this observation, we averaged dissimilarities between different fingers pressing in the same direction (finger-specific) and the same finger pressing in different directions (direction-specific). The finger and direction-specific dissimilarities were close in magnitude for both monkeys (Fig. 5A). Also, the human EMG patterns had roughly matched direction and finger-specific dissimilarities (Fig. 5B). In contrast, the same analysis on the human fMRI data showed a clear and significant difference between these two kinds of dissimilarities (Fig. 5C).

For a statistical comparison, we then calculated the ratio between dissimilarities between different directions and dissimilarities between different fingers (Fig. 5D). The fMRI ratio was significantly lower than 1 (mean ratio=0.298 ±0.071 sem; one-sided one-sample t-test ratio<1: t_8=-4.747, p=0.0015), indicating stronger representation of fingers compared to direction. In contrast, both the spiking patterns (monkey C ratio=1.173, monkey G ratio=1.025) and the human muscle patterns (mean ratio=0.984 ±0.050 sem) differed similarly for different fingers and different directions, with the muscle ratios being significantly larger than those for human fMRI (two-sided paired t-test: t_8=9.804, p=9.840e-6). Thus, we found a clear difference between the structure of fMRI patterns and the structures of spiking and muscle activity patterns. We suggest this difference comes about because fMRI (input activity) and single-cell electrophysiology (spiking of mainly output neurons) reflect two fundamentally different aspects of neuronal activity. The neuronal population controlling flexion and extension may receive very similar input (and therefore show similar fMRI activity patterns), while their output firing must be quite distinct to produce the different patterns of muscle activity required for fine finger control.

bioRxiv preprint doi: https://doi.org/10.1101/2020.03.17.996124; this version posted March 18, 2020. The copyright holder for this preprint (which was not certified by peer review) is the author/funder. All rights reserved. No reuse allowed without permission.

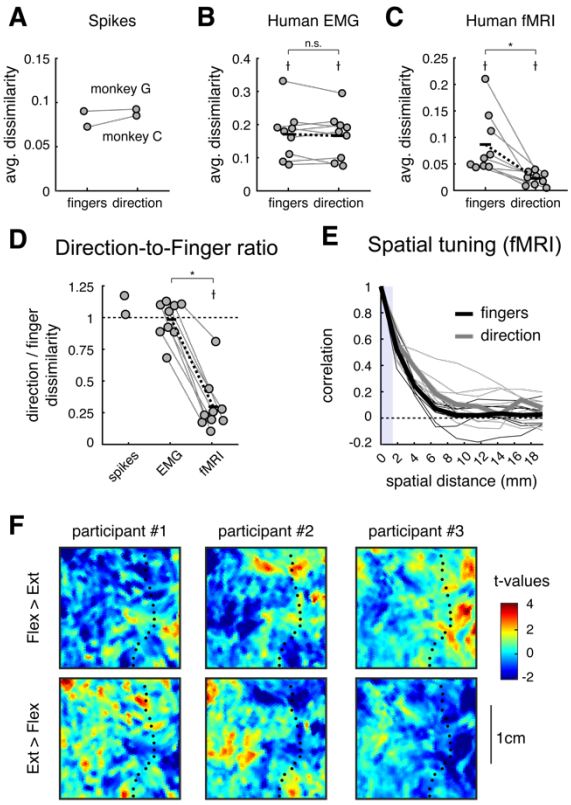

Figure 5 | Comparing strength of finger and direction representations across datasets. The average finger and direction-specific dissimilarities for the spiking (**A**), human EMG (**B**), and human fMRI (**C**) datasets. Each dot denotes one participant, and lines connect dots from the same participants. Black bars denote the means, and black dashed lines reflect the mean paired differences. † dissimilarities significantly larger than zero (one-sided t-test, $p<0.05$). *significant difference between finger and direction dissimilarities (two-sided paired t-test, $p<0.05$). (**D**) The ratio of the direction-to-finger dissimilarities for each dataset. Values <1 indicate stronger finger representation. †dissimilatrities significantly lower than one (one-sided t-test, $p<0.05$). *significiant differences between dissimiarity ratios (two-sided paired t-test, $p<0.05$). (**E**) Estimated spatial autocorrelations of finger (black) and direction (grey) pattern components in human M1, plotted as a function of spatial distance between voxels. No significant difference was observed between finger and direction tuning in M1. The thick lines denote the median spatial autocorrelation functions, and small lines are drawn for each participant for each pattern component. The vertical shaded bar denotes the distance between voxel size, for which correlations can be induced by motion correction. (**F**) Differences between average finger flexion and extension activity maps. We averaged across presses of any finger in the same direction, and calculated the differences. Maps are plotted on the same inset as in figure 1C.

Differences between fMRI and spiking are not explained by different spatial scales of the measurements.

There is another key difference between the fMRI and spiking data set that may explain the discrepancy. That is, fMRI samples a proxy of neuronal activity in a coarse manner, averaging across at least 200,000 cortical neurons per mm^3 in M1 (Young,

bioRxiv preprint doi: https://doi.org/10.1101/2020.03.17.996124; this version posted March 18, 2020. The copyright holder for this preprint (which was not certified by peer review) is the author/funder. All rights reserved. No reuse allowed without permission.

Collins, & Kaas, 2013). Thus, even high-resolution fMRI is biased to functional organization at a coarse spatial scale (Kriegeskorte & Diedrichsen, 2016), and so our results could be caused by an organization where neurons tuned to different movement directions for the same finger (or combination of fingers) are clustered together, while neurons that control different finger or finger combinations are more spatially separated.

To investigate this idea, we correlated the finger-specific and direction-specific activations for each pair of voxels within M1, and binned these correlations according to the spatial distance between voxel pairs (see Methods). If direction is encoded at a finer spatial scale than fingers, we would expect finger effects should be correlated over larger spatial distances.

In contrast to this prediction, the spatial correlation functions for fingers and direction were quite similar (Fig. 5E). We estimated the full-width at half-maximum (FWHM) of the spatial autocorrelation functions. To account for outliers, we evaluated the median FWHMs. The median FWHM of the finger spatial kernel in M1 was 4.55mm (mean=4.87mm ±0.33), comparable to previous reports (Diedrichsen, Ridgway, Friston, & Wiestler, 2011; Wiestler, McGonigle, & Diedrichsen, 2011). The median FWHM of the direction spatial kernel in M1 was 6.57mm (mean=6.75mm ±1.18), and there was no significant difference between the two (two-sided paired Wilcoxon signed-rank test, finger vs. direction: p=0.2031; two-sided paired t-test finger vs. direction: t_8=-1.417, p=0.1942). We also did not find evidence of a clear spatial gradient for flexion vs. extension movements, as was reported by Huber et al. (2020). Areas responding more to flexion or extension were spatially diffuse and could be found across the hand area of M1 (Fig. 5F). Therefore, at least at the spatial scale measurable with 7T fMRI, we did not find any empirical support for the idea that directions are represented at a different spatial scale than fingers in M1.

Discussion

Here we investigated how the population activity in M1 is organized for control of flexion and extension of single fingers. We analyzed M1 population activity measured in humans with 7T fMRI and spiking data from NHPs while participants made isometric single finger presses in either direction. Importantly, we ensured the behavioural tasks in both experiments were carefully matched to allow us to compare results across the two datasets.

We first demonstrated that the representational structure of single finger presses in human M1 were relatively well explained by the statistics of every-day movements, replicating the flexion results reported in Ejaz et al. (2015) and extending them to single

bioRxiv preprint doi: https://doi.org/10.1101/2020.03.17.996124; this version posted March 18, 2020. The copyright holder for this preprint (which was not certified by peer review) is the author/funder. All rights reserved. No reuse allowed without permission.

finger extension movements. The same model, however, failed to correctly predict the relationship between flexion and extension movements. Because flexion and extension of the same finger cannot temporally co-occur, the model predicted quite separate representations for the two actions. In our data, however, we observed the opposite effect – cortical M1 activity patterns measured with fMRI were very similar for the flexion and extension of the same finger, as compared to the quite distinct patterns for different fingers. These findings were specific to fMRI: In the electrophysiological recording, different movement directions were associated with distinct patterns of neuronal activity.

The most likely explanation for this difference comes from the fact that fMRI and electrophysiological recordings measure different physiological processes. In cortical grey matter, the BOLD signal measured with fMRI reflects mainly excitatory postsynaptic potentials (EPSP), caused by input to a region or recurrent activity within a region (Logothetis, Pauls, Augath, Trinath, & Oeltermann, 2001). This is because much of the metabolic costs associated with signal transmission arise from re-establishing resting membrane potential of neurons (Attwell & Laughlin, 2001; Magistretti & Allaman, 2015; Yu, Herman, Rothman, Agarwal, & Hyder, 2018). In contrast, single-cell recordings directly measure action potentials, and are usually biased towards the large output cells in M1 (Firmin et al., 2014).

Figure 6 | Summary model of M1 organization. Output neurons in M1 produce complex patterns of muscular activity. We refer to groups of neurons that, together, evoke a complex pattern of muscle activty that results in single finger movements as functional units (circles). Functional units that evoke movements of the same finger in opposite directions receive common inputs (dashed lines) and share strong recurrent connections (circular lines). The spiking output (solid lines) of these units, however, is directionally specific. The proximity of functional units tuned for the same finger and/or direction is unknown.

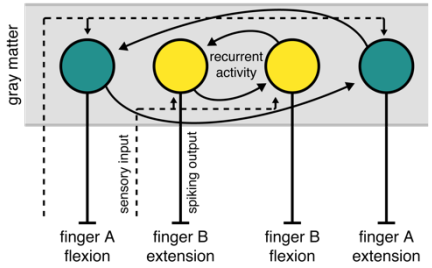

This consideration leads us to a new model of hand movement encoding in M1 (Fig. 6). We hypothesize that neurons that contribute to the flexion of a finger receive similar sensory input as neurons that contribute to the extension of the same finger (dashed line, Fig. 6). This common input would manifest as similar patterns of fMRI activity for flexion and extension for the same finger. There is evidence in the literature to support such an organization. Single neurons tuned to torque production at the shoulder integrate information from the shoulder and elbow joints to facilitate rapid corrective

bioRxiv preprint doi: https://doi.org/10.1101/2020.03.17.996124; this version posted March 18, 2020. The copyright holder for this preprint (which was not certified by peer review) is the author/funder. All rights reserved. No reuse allowed without permission.

responses to mechanical arm perturbations (Pruszynski et al., 2011). Thus, these neurons receive common sensory input about the shoulder and elbow joints, but the output is largely specific to movements about the shoulder.

Additionally, it is also likely that units controlling flexion and extension of the same finger directly communicate with each other (solid arrows, Fig. 6). Such coordination would be necessary to orchestrate fast alternation of finger movements or to finely control the grip force during object manipulation. The resultant recurrent cortical activity would again make the fMRI activity patterns for flexion and extension more similar (Fig. 1C).

If units controlling muscle patterns that produce flexion and extension of the same effector have to closely communicate with each other, it might be that they are spatially co-localized to support fast and efficient communication. This would predict that differences between fingers should be on a courser spatial scale than differences between directions, which may explain why differences between fingers were more clearly detectable with fMRI. We did not find any evidence for a difference in spatial organization of fingers and direction in the fMRI data. However, given that this comparison itself is limited by the spatial resolution of fMRI, we cannot rule out that differences in the fine-grained spatial organization also contributed to the observed effect.

Although we experimentally studied the flexion and extension of single fingers, we do not suggest that isolated finger movements are explicitly represented in M1. Rather, M1 output neurons will produce a complex pattern of muscle activity. This complexity likely arises because the neuronal populations are optimized to produce combinations of muscle activities which elicit finger movements that are useful in everyday tasks (Poliakov & Schieber, 1999; Gentner & Classen, 2006; Ejaz et al., 2015). When we measure activity patterns related to movements of isolated fingers, we simply observe the specific combination of neuronal populations that need to be active to move a single finger (Schieber, 1990). The core of our hypothesis is that population of neurons that produce opposing muscular patterns communicate closely with each other and also receive similar sensory input.

Our findings are at odds with the organization suggested by Huber et al. (2020). Using high-resolution functional imaging, the authors reported evidence of multiple single-finger representations along the lateral-medial axis of M1, arranged into two spatially distinct maps, one for flexion and one for extension. While we found clear evidence that each single finger press actives multiple patches in M1 (Fig. 1C), we did not find any evidence for a systematic spatial separation of flexion and extension maps

bioRxiv preprint doi: https://doi.org/10.1101/2020.03.17.996124; this version posted March 18, 2020. The copyright holder for this preprint (which was not certified by peer review) is the author/funder. All rights reserved. No reuse allowed without permission.

(Fig 5F). We do not think that this is an issue of experimental power: Although we used a slightly lower resolution in our study, we should have been able to detect the organisation proposed by Huber et al. (2020). Instead, the differences are likely explained by the fact that Huber et al. did not study flexion and extension of individual fingers, but relied on large spatial gradients detected between whole-hand grasping and retraction, which may have involved neuronal populations that are not normally engaged during fine finger movements (Muir & Lemon, 1983).

Indeed, there are two lines of evidence that argue against a spatial separation of individuated flexion and extension actions. First, electrophysiological recordings from M1 also show that flexion and extension preference is not spatially clustered (Schieber & Hibbard, 1993). Second, partial inactivation of neurons in the hand area of M1 results in a complex loss of flexion and/or extension movements of different fingers (Schieber & Poliakov, 1998), demonstrating that different directions of movement are not likely to be encoded in spatially clustered action maps.

There are of course many caveats when comparing results across different recording methodologies, experimental setups, and species. While we tried to make the behavioural tasks across human and macaques as similar as possible, species differences or the extensive training for the non-human primates may account for some of the differences.

Overall, however, we believe that the comparison between fMRI and spiking provides some interesting insights into the organization of the hand region of the primary motor cortex. Cortical representations of single finger movements are not purely dictated by the kinematics of hand usage. We posit that the deviation from this organization appears to reflect a control process, where neurons tuned to movements of a specific finger receive common sensory input and share local recurrent processes. These tightly coordinated populations then produce the spiking output that needs to be quite distinct for the flexion and extension of the same finger.

bioRxiv preprint doi: https://doi.org/10.1101/2020.03.17.996124; this version posted March 18, 2020. The copyright holder for this preprint (which was not certified by peer review) is the author/funder. All rights reserved. No reuse allowed without permission.

Methods

Human participants

Nine healthy, participants were recruited for the study (5 males and 4 females, mean age=24.78, SD=4.68; mean Edinburgh handedness score=90.11, SD=11.34). Participants completed 3 experimental sessions. During the first training session, participants learned to perform the finger individuation task. In the scanner session, participants performed the finger individuation task while undergoing fMRI. In the EMG session, participants performed the finger individuation task while muscle activities were recorded. All participants provided informed consent before the beginning of the study, and all procedures were approved by the Office for Research and Ethics at the University of Western Ontario.

Human finger individuation task

In all three sessions, the five fingers of the right hand were individually clamped between two keys (Fig. 1A). Foam padding on each key ensured each finger was comfortably restrained. Force transducers (Honeywell-FS series, dynamic range=0-16N, resolution<0.02N, sampling rate=200Hz) above and below each key monitored the forces applied by each finger in extension and flexion directions.

During the task, participants viewed a screen that presented two rows of five bars (Fig. 1B). These bars corresponded to flexion or extension direction for each of the five fingers of the right hand. The forces applied by each finger were indicated on the visual display as five solid white lines (one per finger). On each trial, participants were cued to make an isometric, single-finger flexion or extension press at one of three forces levels (1, 1.5, or 2N for extension; 1.5, 2, or 2.5N for flexion) through the display of a white target box (Fig. 1B). Extension forces were chosen to be lower than flexion forces, as extension finger presses are more difficult (Valero-Cuevas, Zajac, & Burgar, 1998; Li, Pfaeffle, Sotereanos, Goitz, & Woo, 2003) and can lead to more enslaving (i.e. co-articulation) of non-instructed fingers (Yu, Duinen, & Gandevia, 2010). The forces were similar to the low forces required in the monkey task design. The finger displacement required to achieve these force thresholds was minimal, such that the finger presses were close to isometric.

Each trial lasted 6000ms and consisted of four phases (Fig. 1B): a cue phase (1500ms), a press phase (2000ms), a hold phase (1000ms), and a 1500ms inter-trial interval. This trial structure was designed to mirror the NHP task (see NHP methods; Schieber, 1991). During the cue phase, a white box appeared in one of the ten finger bars presented on screen, indicating the desired finger and direction. The

bioRxiv preprint doi: https://doi.org/10.1101/2020.03.17.996124; this version posted March 18, 2020. The copyright holder for this preprint (which was not certified by peer review) is the author/funder. All rights reserved. No reuse allowed without permission.

desired pressing force was reflected by the relative location of the cue within the finger bar. After 1500ms, the cue turned green. This instructed the participant to initiate the finger press. Participants had up to 2000ms after the cue turned green to reach the specified force. Once the pressing force was within the target box (target force ±12.5%) the cue turned blue. Participants were trained to hold the force constant within this interval for 1000ms. When this time had elapsed, the cue disappeared and the participants were instructed to release the press by relaxing their hand. Importantly, participants were instructed not to actively move the finger in the opposite direction. A new trial started every 6s. For the scanning session, periods of rest were randomly intermixed between trials (see below). The muscle recording sessions lacked these rest periods, but otherwise had the same trial structure.

Trials of the 30 conditions (5 fingers x 2 directions x 3 forces) were presented in a pseudo-random order. Trials were marked as incorrect if the participant was too slow (i.e. did not initiate movement within 2000ms of the go-cue) or if the participant did not reach at least 0.5N force with the cued finger in the cued direction. Due to the pre-training, the participants had low error rates in both the fMRI (mean error rate=1.48% ±1.05% sem) and EMG (mean error rate=1.30% ±0.97%) sessions, and accurately produced the required forces (fMRI: mean peak force accuracy=108.37% ±2.67% of the target forces; EMG: mean accuracy=107.11% ±2.21%). Therefore, we included all trials in our analyses.

We also did not exclude any trials based on finger co-activation. Overall, participants were able to individuate their fingers relatively well. During fMRI extension trials, the forces applied through the non-instructed fingers were, on average, 12.083% (±1.489%) of the forces applied by the instructed finger. During fMRI flexion, forces produced by on non-instructed fingers was 19.761% (±1.713%) of the force produce by the instructed finger. Most enslaving occurred during presses of the middle, fourth, and little fingers, all of which are difficult to individuate (Schieber, 1991). Note, however, that the presence of enslaving does not compromise the main finding of our paper. To some degree, neural activity patterns related to flexion and extension of single fingers will always depend on the biomechanical coupling between fingers, either because the cortical activation patterns need to overcome that coupling, or because coupling does occur, which then influences the recurrent sensory input. Our main conclusions are based on comparisons between flexion and extension presses, and remain valid whether we study the actions of isolated fingers, or groups of fingers (see discussion).

fMRI data acquisition

bioRxiv preprint doi: https://doi.org/10.1101/2020.03.17.996124; this version posted March 18, 2020. The copyright holder for this preprint (which was not certified by peer review) is the author/funder. All rights reserved. No reuse allowed without permission.

We used high-field functional magnetic resonance imaging (fMRI, Siemens 7T Magnetom with a 32 channel head coil at Western University, London, Ontario, Canada) to measure the blood-oxygen-level dependent (BOLD) responses in human participants. For each participant, evoked-BOLD responses were measured for isometric, single-finger presses in the flexion and extension directions.

There were 2 repeats of each condition during each imaging run (5 fingers × 2 directions × 3 force levels × 2 repeats = 60 trials). Trial order in each run was randomized. In addition, 5 rest conditions of 6000ms were randomly interspersed between trials within each run. Each run lasted approximately 390 seconds. Participants performed 8 such runs during the scanning session.

During each run, 270 functional images were obtained using a multiband 2D-echoplanar imaging sequence (GRAPPA, in-plane acceleration factor=2, multi-band factor=2, repetition time [TR]=1500ms, echo time [TE]=20ms, flip angle [FA]=45 deg). Per image, we acquired 32 interleaved slices (without gap) with isotropic voxel size of 1.5mm. The first 2 images in the sequence were discarded to allow magnetization to reach equilibrium. To estimate magnetic field inhomogeneities, we acquired a gradient echo field map at the end of the scanning session. Finally, a T1-weighted anatomical scan was obtained using a magnetization-prepared rapid gradient echo sequence (MPRAGE) with a voxel size of 0.75mm isotropic (3D gradient echo sequence, TR=6000ms, 208 volumes).

fMRI image preprocessing and first-level analysis

Functional images were first realigned to correct for head motion during the scanning session (3 translations: x,y,z; 3 rotations: pitch, roll, yaw), and co-registered to each participant's anatomical T1-image. Within this process, we used a B0 fieldmap to correct for image distortions arising from magnetic field inhomogeneities (Hutton et al., 2002). No slice-timing correction was applied due to the relatively short TR. The data were not smoothed or normalized to a standard template.

The minimally preprocessed data were then analyzed using a general linear model (GLM; Friston et al., 1994) using SPM12 (fil.ion.ucl.ac.uk/spm/). Each of the finger-direction-force conditions were modeled with separate regressors per run, resulting in 30 regressors per run (30*8 runs = 320 task regressors), along with an intercept for each run. The regressor was a boxcar function that started at the presentation of the go-cue and lasted for the trial duration, spanning the press, hold, and release periods of each trial. The boxcar functions were convolved with a hemodynamic response function with a delayed onset of 1000ms and a post-stimulus undershoot at 7500ms. Given the low

bioRxiv preprint doi: https://doi.org/10.1101/2020.03.17.996124; this version posted March 18, 2020. The copyright holder for this preprint (which was not certified by peer review) is the author/funder. All rights reserved. No reuse allowed without permission.

error rate (Supplementary Table 2), we did not exclude any trials from this analysis. We used the SPM FAST autocorrelation model with restricted-maximum likelihood estimation to model the long-range temporal dependencies in the functional timeseries (see Arbuckle et al., 2019 for details). This analysis resulted in one activation estimate ("beta-weights") for each of the 30 conditions per run for each participant.

Surface reconstruction and region of interest definitions

Each participant's T1-image was used to reconstrct the pial and white-grey matter surfaces using Freesurfer (Fischl, Sereno, & Dale, 1999). Individual surfaces were aligned across participants and spherically registrated to match a template atlas (Fischl, Sereno, Tootell, & Dale, 1999) using a sulcal-depth map and local curvatuer as minimization criteria. M1 was defined as a single region of interest (ROI) on the group surface using probabilistic cuto-architectonic maps aligned to the template surface (Fischl et al., 2008). We defined M1 as being the surface nodes with the highest probability for Brodmann area 4 and who fell within 2cm above and below the hand knob anatomical landmark (Yousry et al., 1997). To avoid cross-contamination between M1 and S1 activities along the central sulcus, voxels with more than 25% of their volume in the grey matter on the opposite side of the central sulcus were excluded.

Multivariate fMRI analysis

We used the cross-validated Euclidean (crossnobis) dissimilarity to quantify differences between fMRI activity patterns for each pressing condition within each participant (Walther et al., 2016). Cross-validation ensures the distances estimates are unbiased, such that if two patterns differ only by measurement noise, the mean of the estimated value would be zero. This also means that estimates can sometimes become negative (Diedrichsen, Provost, & Zareamoghaddam, 2016). Therefore, dissimilarities significantly larger than zero indicate that two patterns are reliably distinct.

The distances are organized in a representational dissimilarity matrix (RDM). The RDM is a symmetric matrix (number of conditions x number of conditions in size) with off-diagonal values corresponding to the paired distance between two conditions. Values along the diagonal are zero, as there is no difference between a pattern paired with itself.

The fMRI activity patterns were first-level GLM parameter estimates ("beta-weights") for voxels within the M1 ROI mask. Analyses were conducted using functions from the RSA (Nili et al., 2014) and PCM (Diedrichsen, Yokoi, & Arbuckle, 2018) MATLAB toolboxes. The M1 beta-weights were first spatially pre-whitened using multivariate noise-normalization with a regularized estimate of the spatial noise-covariance matrix to

bioRxiv preprint doi: https://doi.org/10.1101/2020.03.17.996124; this version posted March 18, 2020. The copyright holder for this preprint (which was not certified by peer review) is the author/funder. All rights reserved. No reuse allowed without permission.

suppress correlated noise across voxels (Walther et al., 2016). Then, the mean pattern across-conditions was removed from each run independently. Finally, we calculated the crossnobis dissimilarity between pairs of fMRI activity patterns for different conditions:

$$d_{i,j} = \left(x_i - x_j\right)_A^T \Sigma_A^{-\frac{1}{2}} \Sigma_B^{-\frac{1}{2}} \left(x_i - x_j\right)_B$$

where d is the dissimilarity between activity patterns of conditions i and j in run A, and Σ is the voxel-wise noise covariance matrix. We calculated an RDM for the matched force conditions separately (1.5N and 2N presses, 10 conditions each), and then averaged the resulting RDMs within each participant. This yeilded one RDM per participant containing the dissimilarities between presses of the five fingers in either direction (10 conditions, 45 dissimilarity pairs).

Estimating spatial tuning of fingers and direction

For the spatial tuning analysis, we estimated the spatial covariance of tuning for fingers and directions. To do this, we first univariately prewhitened the fMRI activity patterns (multivariate prewhitening would partly remove the spatial tuning we are attempting to measure). To remove the influence of noise on the covariance estimate, we then partitioned the data in two according to odd or even number imaging runs. Within each partition, we averaged the fMRI activity patterns for each condition across the matched forces (1.5 and 2N). This yielded a vector of 10 activity values per voxel per partition (5 flexion, 5 extension), which we refer to as an *activity profile*. For each voxel, we then mean-centered the activity profile.

Per partition (k), we modeled the activity profile of each voxel (y) using three components: a main effect of fingers (f), a main effect of direction (d), and a finger x direction interaction effect (q):

$$y_k = f_k + d_k + q_k$$

We then used these components to reconstruct the activity profiles of each voxel, including finger or direction components accordingly.

We first investigated the spatial tuning for fingers across voxels in M1. To do this, we reconstructed the activity profiles using only the finger component (f). Across voxels, the reconstructed finger activity profiles explained, an average, 60% of the full activity profiles (evaluated as R^2). We then estimated the covariance of the finger activity profiles between voxel pairs in M1. This was done in a cross-validated fashion, comparing voxel pairs across the two partitions. We then binned the covariances based on the spatial distance between each voxel pair. The first bin included immediately and diagonally neighbouring voxels (1.5 to 2.6mm), the second bin the second layer of direct and diagonally neighbouring voxels (>2.6 to 5.2mm), and so on, up to a total distance of

bioRxiv preprint doi: https://doi.org/10.1101/2020.03.17.996124; this version posted March 18, 2020. The copyright holder for this preprint (which was not certified by peer review) is the author/funder. All rights reserved. No reuse allowed without permission.

20.8mm. Finally, we normalized the binned covariances by the cross-validated voxel variances to obtain an estimate of the spatial autocorrelation function (ACF) for fingers in M1.

We used the same procedure to estimate the ACF for direction. Importantly, we included both the direction (d) and the finger x direction interaction (q) components in the activity profile reconstruction. We included the interaction component as we hypothesized that the tuning of voxels to flexion and extension patterns would be different across fingers. Across voxels, these reconstructed direction activity profiles explained, on average, 40% of the variance of the full activity profiles.

Finally, we estimated the smoothness of the finger and direction ACFs (Diedrichsen, Ridgway, Friston, & Wiestler, 2011). To do this, we fitted a function that decayed exponentially with the square of the distance (δ) between two voxels:

$$ACF(v_x, v_{x+\delta}) = \exp\left(-\frac{\delta^2}{2s^2}\right)$$

Here, s is the standard deviation of the ACF. If neighbouring voxels are relatively independent (i.e. low covariance), the value of s will be small. While we can use s to express the smoothness of the ACF, the smoothness can also be expressed as the full-width-half-maximum (FWHM) of the Gaussian smoothing kernel that- when applied to spatially independent data- would yield the same ACF. The FWHM is thus more readily interpretable. The FWHM of this Gaussian kernel is calculated as:

$$FWHM = 2s\sqrt{2\log(2)}$$

We applied this approach to the reconstructed finger and direction activity profiles separately to estimate the FWHM of fingers and direction M1. The goodness of fit (evaluated with R^2) of the fitted exponential decays were not significantly different between the finger and direction models (mean R^2 of finger ACF=0.978, mean R^2 of direction ACF=0.980; two-sided paired t-test: t_8=0.189, p=0.8547).

EMG muscle recordings

Participants' skin was cleaned with rubbing alcohol. Surface EMG of distal muscles of the hand were recorded with self-adhering Ag/AgCl cloth electrodes (H59P-127 repositionable monitoring electrodes, Kendall, Mansfield, Massachusetts, USA). Electrodes were cut and positioned in line with a muscle in a bi-polar configuration with an approximate 1cm inter-electrode distance. Surface EMG of proximal limb muscles were recorded with surface electrodes (Delsys Bagnoli-8 system with DE-2.1 sensors). The contacts were coated with a conductive gel. Ground electrodes were placed on the

bioRxiv preprint doi: https://doi.org/10.1101/2020.03.17.996124; this version posted March 18, 2020. The copyright holder for this preprint (which was not certified by peer review) is the author/funder. All rights reserved. No reuse allowed without permission.

ulna at the wrist and elbow. The signal from each electrode was sampled at 2000Hz, de-meaned, rectified, and low-pass filtered (fourth order butterworth filter, f_c=40Hz).

Multivariate EMG analysis

We used the cross-validated Euclidean (crossnobis) distance to quantify differences between patterns of muscle activities for each movement condition, similar to the fMRI analysis. This metric is invariant to scaling of the EMG signals from each electrode, and has been established in previous work (Ejaz et al., 2015). Briefly, we first calculated the average square-root EMG activity for each electrode and trial by averaging over the press and hold time windows (mean window= 1800ms, up to a max window of 3000ms). We then subtracted the mean value for each electrode across conditions for each run independently to remove any drifts in the signal. These values were then divided by the standard deviation of that electrode across trials and conditions to avoid arbitrary scaling. Finally, we calculated the crossnobis dissimilarity between pairs of EMG activity patterns for different conditions across runs.

Monkey finger individuation task

The behavioural task performed by two *Macaca mulatta* monkeys (monkeys C and G) has been described previously (Schieber, 1991; Schieber & Rivlis, 2007). Briefly, the monkeys were trained to perform cued single finger flexion and extension presses. Each monkey sat in a primate chair and, similar to the human device described above, their right hand was clamped in a device that separated each finger into a different slot (Fig. 7A). Each slot was comprised of two microswitches (one in the flexion direction and one in the extension direction). One switch was closed by flexing the finger, the other by extending the finger. The absolute degree of movement required to close either switch was minimal (a few millimeters), and therefore the force required to make and hold a successful press was small- similar to the human finger individuation task. Therefore, like the fMRI task behaviour, these finger movements are very close to isometric presses.

A series of LED instructions were presented to the monkey during each trial (Fig. 7B). A successful trial occurred when the monkey pressed the cued finger in the cued direction without closing any other switch. Similar to our human experiment design, the monkeys were trained to hold the cued switch closed for 500ms, before relaxing the finger (Fig. 7C). At the end of a successful trail, the monkey received a water reward. The monkey's wrist was also clamped in this device, and some trials required the monkey to flex or extend the wrist. Wrist trials were not included in the current analysis. Flexion and extension trials of each finger and wrist were pseudorandomly ordered. In the case of a behavioural error, trials were repeated until successful. Therefore, we excluded the

bioRxiv preprint doi: https://doi.org/10.1101/2020.03.17.996124; this version posted March 18, 2020. The copyright holder for this preprint (which was not certified by peer review) is the author/funder. All rights reserved. No reuse allowed without permission.

successful trials that followed error trials to avoid potential changes in the baseline firing rate of the recorded neuron.

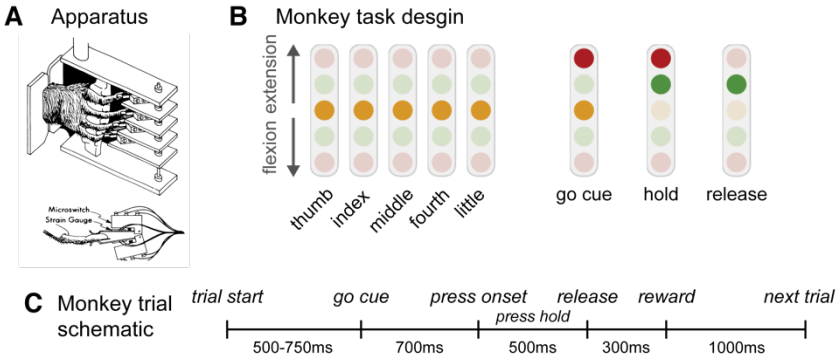

Figure 7 | **Monkey finger individuation task.** (**A**) The monkey hand configuration and device (illustration from Schieber, 1991). (**B**) Visual feedback for the NHP task. The columns represent 5 LED cues for each finger that instructed the monkey both what finger and what direction to press. (**C**) A trial schematic for the monkey finger individuation task. The monkeys had up to 700ms from the onset of the go cue to press the cued finger in the cued direction. They were trained to hold the press for 500ms before relaxing the finger.

Spike rate calculation

Single cells were isolated and spike times were recorded while monkeys performed the finger individuation task. The details of the recordings are reported previously (Schieber & Poliakov, 1998). Each trial was labeled with a series of behavioural markers, indicating the time of trial onset, presentation of condition cue, switch closure, and reward onset. For the spike rate traces plotted in Figure 4, we calculated the spike rate per 10ms bin, aligned to press onset, and smoothed the binned rates with a Gaussian kernel (FWHM=50ms). For the dissimilarity analysis (see below), we calculated the average spike rate over time per trial starting at go cue onset (when the monkey was instructed as to which finger and direction to press) until the end of the hold phase (500ms after switch closure). This time window encompassed a short period of time prior to the start of the finger press and the entire hold duration of the press (Monkey C: mean window= 739ms; Monkey G: mean window=773ms).

Multivariate spiking analysis

Similar to the human fMRI and EMG analyses, we computed crossnobis distances between spiking patterns for different conditions within each monkey. To cross-validate the estimated distances, we restricted our analysis to include cells for which we had at least two successful trials for each finger in both directions (238 cells in monkey C and 45 cells in monkey G). After calculating the average spike rates, we arranged the spike rates into vectors per condition (Fig. 4B). In order to account for the Poisson-like increase

bioRxiv preprint doi: https://doi.org/10.1101/2020.03.17.996124; this version posted March 18, 2020. The copyright holder for this preprint (which was not certified by peer review) is the author/funder. All rights reserved. No reuse allowed without permission.

of variability with increasing mean firing rates, we applied the square-root transform to the average firing rates (Yu et al., 2009).

For each cell per condition, we randomly split the square-root spike rates into one of two partitions, ensuring that each trail was approximately equally represented in each partition. We then averaged the spike rates within each partition. This yielded two independent sets of spiking patterns per monkey (10 patterns- 5 fingers x 2 directions). Per partition, we normalized each neuron's spike pattern by dividing by the neuron's max rate across conditions, and then re-weighted the spike rates per cell according to the number of trials per cell (cells with more trials were up-weighted, vice versa for cells with fewer trials). Finally, we calculated pairwise cross-validated Euclidean distances between the two sets of patterns. We repeated this RDM calculation procedure 1000x per monkey, each time using a different random partitioning of the data. We then averaged the RDMs across iterations to yield one RDM estimate per monkey. We note that results were qualitatively consistent across a range of different pre-processing approaches (e.g. using raw spike rates, z-scoring the firing rates, not applying trial re-weighting).

Kinematic finger model RDM

As in Ejaz et al. (2015), we used the statistics of naturalistic hand movements to predict the relative similarity of single finger representations in M1. In the text we refer to this model as the kinematic model. To construct the kinematic model RDM, we used hand movement statistics from an independent study in which 6 male participants wore a cloth glove imbedded with motion sensory (CyberGlove, Virtual Technologies) while they performed everyday activities (Ingram, Körding, Howard, & Wolpert, 2008). These statistics included the velocities about joint angles specific to each of the five fingers of the participants' right hands. Positive velocities indicated finger flexion, and negative velocities indicated finger extension.

Because the movement in our finger pressing task was restricted to movements about the metacarpal (MCP) joint of each finger, we used the MCP joint velocities to predict cortical M1 finger similarity. First, we split the data for each joint velocity into two vectors: one for flexion and one for extension, taking the absolute of the velocities in this process. During periods of finger flexion, we set the extension velocity to zero, and vice versa. This resulted in 10 velocity vectors (5 fingers x 2 directions). Then, to account for differences in scaling, we normalized each velocity vector to a length of 1. Finally, we calculated the dissimilarities between pairs of these processed velocity vectors. We

bioRxiv preprint doi: https://doi.org/10.1101/2020.03.17.996124; this version posted March 18, 2020. The copyright holder for this preprint (which was not certified by peer review) is the author/funder. All rights reserved. No reuse allowed without permission.

averaged these RDMs across the six participants in the natural statistics dataset, yielding one kinematic model RDM.

Statistical analysis of dissimilarities

We summarized the RDMs by classifying dissimilarities into finger-specific and direction-specific dissimilarities for each participant and dataset. Finger-specific dissimilarities were the dissimilarities between conditions where different fingers were pressed in the same direction (10 pairs for flexion, 10 pairs for extension). Direction-specific dissimilarities were the dissimilarities between conditions where the same finger was pressed in different directions (5 pairs total). Within each category, dissimilarities were averaged. To compare between the average finger and direction dissimilarities, we used two-sided paired t-tests. We report the mean and standard error of the dissimilarities where appropriate in the text.

Statistical analysis of RDM correlations

Pearson's correlations between the vectorized upper-triangular elements of the RDMs were used to compare different RDMs. To calculate the stability of RDMs, we calculated the Pearson's correlations between all possible pairs of the participants' RDMs. This yielded 36 correlations (one per unique participant pair). We Fisher-Z transformed these correlations and calculated the mean and standard error. We used these values to calculate the lower and upper bounds of the 95% confidence interval, assuming normality. Finally, the mean and confidence bounds were transformed back to correlations. We report these values in the text as r=mean [lower bound - upper bound]. The same method was applied to correlations between measured RDMs and model predictions. T-tests were performed on Fisher-z transformed correlations.

Estimating noise ceiling for model fits

Since the dissimilarities between fMRI patterns can only be estimated with noise, even a perfect model fit would not result in a perfect correlation with the RDM of each participant. Therefore, we estimated the *noise ceiling*, which places bounds on the expected model correlations if the model is a perfect fit. We first calculated the average correlation of each participant's RDM with the group mean RDM (Nili et al., 2014), treating the mean RDM as the perfect model. The resulting average correlation is an overestimate of the best possible fit, as each RDM is correlated with a mean that includes that RDM (and hence also the measurement error of that RDM). To then estimate a lower bound, we calculated the correlation between a participant's RDM and the group mean RDM in which that individual was removed.

bioRxiv preprint doi: https://doi.org/10.1101/2020.03.17.996124; this version posted March 18, 2020. The copyright holder for this preprint (which was not certified by peer review) is the author/funder. All rights reserved. No reuse allowed without permission.

Supplementary figures

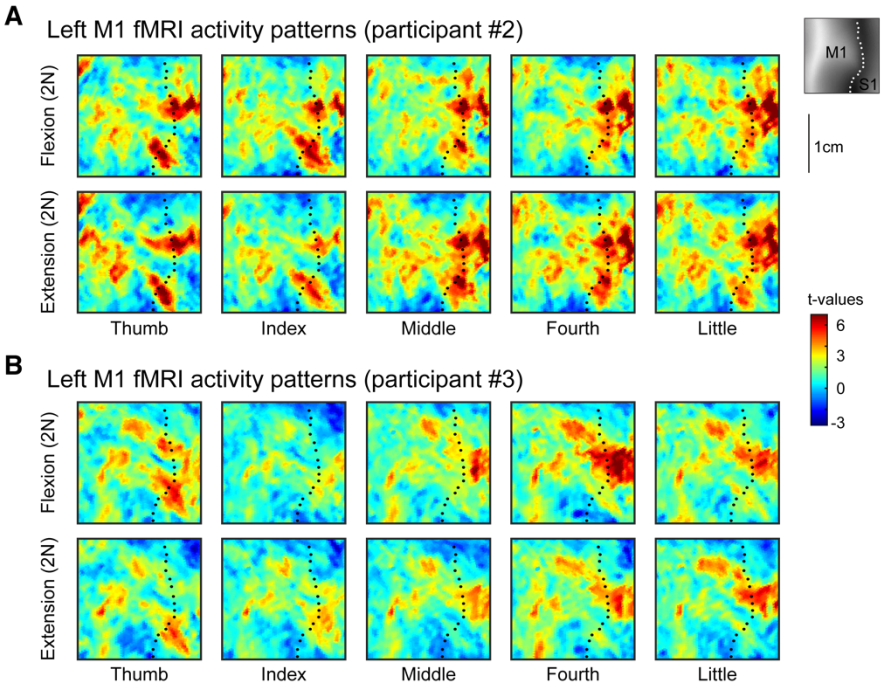

Figure S1 | **fMRI activity maps.** Maps are shown in the hand-knob region of the left (contralateral) hemisphere during 2N presses for participants 2 (**A**) and 3 (**B**). The black dotted line shows the fundus of the central sulcus. There is considerable inter-subject variability of the spatial arrangement of these patterns.

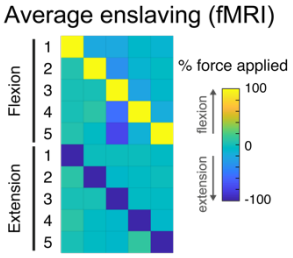

Figure S2 | **Finger enslavement in fMRI task.** Finger enslaving (i.e. forces applied by non-instructed finger) during the fMRI task. Enslavement is expressed as a % of the force that was applied by the cued finger. Positive (negative) values indicate flexion (extension) forces.

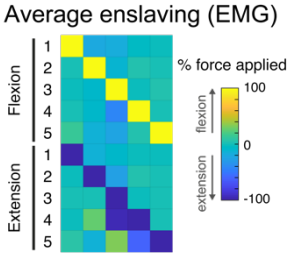

Figure S3 | **Finger enslavement in EMG task.** Finger enslaving (i.e. forces applied by non-instructed finger) during the EMG task. Enslavement is expressed as a % of the force that was applied by the cued finger. Positive (negative) values indicate flexion (extension) forces.

bioRxiv preprint doi: https://doi.org/10.1101/2020.03.17.996124; this version posted March 18, 2020. The copyright holder for this preprint (which was not certified by peer review) is the author/funder. All rights reserved. No reuse allowed without permission.

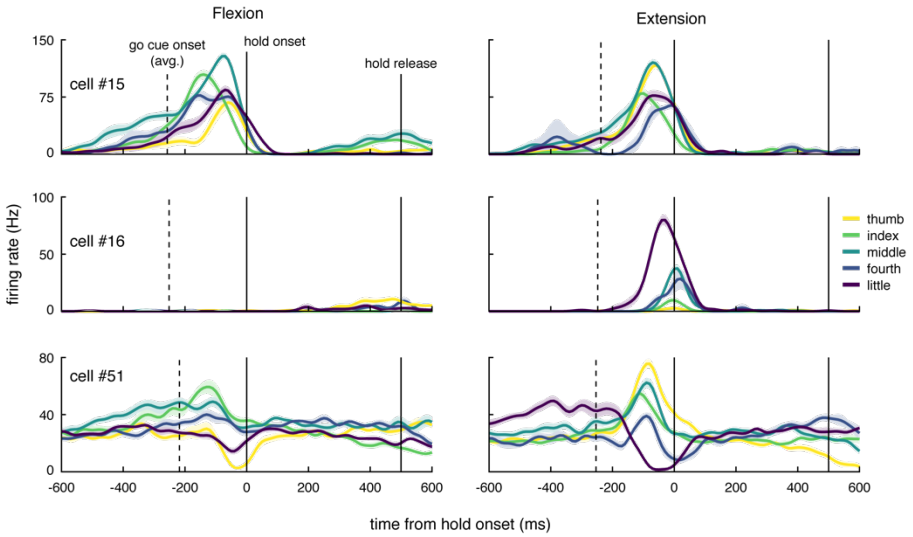

Figure S4 | **M1 spiking activity during monkey single finger flexion and extension.** Trial averaged firing rates from three cells (monkey C). Traces are aligned to press onset (0ms). These cells demonstrate a range of tunings, some finger-specific, some direction-specific, and some mixed. Firing rates were calculated for 10ms bins and smoothed with a gaussian kernel (FWHM=50ms).

bioRxiv preprint doi: https://doi.org/10.1101/2020.03.17.996124; this version posted March 18, 2020. The copyright holder for this preprint (which was not certified by peer review) is the author/funder. All rights reserved. No reuse allowed without permission.

References

Arbuckle, S. A., Yokoi, A., Pruszynski, J. A., & Diedrichsen, J. (2019). Stability of representational geometry across a wide range of fMRI activity levels. *Neuroimage, 186*, 155-163.

Attwell, D., & Laughlin, S. B. (2001). An energy budget for signaling in the grey matter of the brain. *J. Cereb. Blood Flow Metab., 21*, 1133-1145.

Bortoff, G. A., & Strick, P. L. (1993). Corticospinal terminations in two new-world primates: further evidence that corticomotoneuronal connections provide part of the neural substrate for manual dexterity. *J. Neurosci., 13*, 5105-5118.

Darling, W. G., Pizzimenti, M. A., Rotella, D. L., Peterson, C. R., Hynes, S. M., Ge, J., . . . Morecraft, R. J. (2009). Volumetric effects of motor cortex injury on recovery of dexterous movements. *Exp. Neurol., 220*, 90-108.

Diedrichsen, J., Provost, S., & Zareamoghaddam, H. (2016). On the distribution of cross-validated Mahalanobis distances. *arXiv*.

Diedrichsen, J., Ridgway, G. R., Friston, K. J., & Wiestler, T. (2011). Comparing the similarity and spatial structure of neural representations: a pattern-component model. *Neuroimage, 55*, 1665-1678.

Diedrichsen, J., Yokoi, A., & Arbuckle, S. A. (2018). Pattern component modeling: A flexible approach for understanding the representational structure of brain activity patterns. *NeuroImage, 180*, 119-133.

Ejaz, N., Hamada, M., & Diedrichsen, J. (2015). Hand use predicts the structure of representations in sensorimotor cortex. *Nat. Neurosci., 18*, 1034-1040.

Firmin, L., Field, P., Maier, M. A., Kraskov, A., Kirkwood, P. A., Nakajima, K., . . . Glickstein, M. (2014). Axon diameters and conduction velocities in the macaque pyramidal tract. *J. Neurophysiol., 112*, 1229-1240.

Fischl, B., Rajendran, N., Busa, E., Augustinack, J., Hinds, O., Yeo, B. T., . . . Zilles, K. (2008). Cortical folding patterns and predicting cytoarchitecture. *Cereb. Cortex, 18*, 1973-1980.

Fischl, B., Sereno, M. I., & Dale, A. M. (1999). Cortical surface-based analysis. II: Inflation, flattening, and a surface-based coordinate system. *Neuroimage, 9*, 195-207.

Fischl, Sereno, M. I., Tootell, R. B., & Dale, A. M. (1999). High-resolution intersubject averaging and a coordinate system for the cortical surface. *Hum. Brain Mapp., 8*, 272-284.

Friston, K. J., Jezzard, P., & Turner, R. (1994). Analysis of functional MRI time-series. *Human Brain Mapping, 1*, 153-171.

Gentner, R., & Classen, J. (2006). Modular organization of finger movements by the human central nervous system. *Neuron, 52*, 731-742.

Graziano, M. S., & Aflalo, T. N. (2007). Mapping behavioral repertoire onto the cortex. *Neuron, 56*, 239-251.

Heffner, R. S., & Masterton, R. B. (1983). The role of the corticospinal tract in the evolution of human digital dexterity. *Brain Behav. Evol., 23*, 165-183.

Huber, L., Finn, E. S., Handwerker, D. A., Bönstrup, M., Glen, D. R., Kashyap, S., . . . Bandettini, P. A. (2020). Sub-millimeter fMRI reveals multiple topographical digit representations that form action maps in human motor cortex. *Neuroimage, 208*, 116463.

bioRxiv preprint doi: https://doi.org/10.1101/2020.03.17.996124; this version posted March 18, 2020. The copyright holder for this preprint (which was not certified by peer review) is the author/funder. All rights reserved. No reuse allowed without permission.

Hutton, C., Bork, A., Josephs, O., Deichmann, R., Ashburner, J., & Turner, R. (2002). Image distortion correction in fMRI: A quantitative evaluation. *Neuroimage, 16*, 217-240.

Ingram, J. N., Körding, K. P., Howard, I. S., & Wolpert, D. M. (2008). The statistics of natural hand movements. *Exp. Brain Res., 188*, 223-236.

Kriegeskorte, N., & Diedrichsen, J. (2016). Inferring brain-computational mechanisms with models of activity measurements. *Philos. Trans. R. Soc. Lond. B Biol. Sci., 371*.

Lang, C. E., & Schieber, M. H. (2003). Differential impairment of individuated finger movements in humans after damage to the motor cortex or the corticospinal tract. *J. Neurophysiol., 90*, 1160-1170.

Lawrence, D. G., & Hopkins, D. A. (1976). The development of motor control in the rhesus monkey: evidence concerning the role of corticomotoneuronal connections. *Brain, 99*, 235-254.

Lawrence, D. G., & Kuypers, H. G. (1968). The functional organization of the motor system in the monkey. I. The effects of bilateral pyramidal lesions. *Brain, 91*, 1-14.

Lemon, R. N. (2008). Descending pathways in motor control. *Annu. Rev. Neurosci., 31*, 195-218.

Li, Z.-M., Pfaeffle, H. J., Sotereanos, D. G., Goitz, R. J., & Woo, S. L.-Y. (2003). Multi-directional strength and force envelope of the index finger. *Clin. Biomech., 18*, 908-915.

Liu, Y., & Rouiller, E. M. (1999). Mechanisms of recovery of dexterity following unilateral lesion of the sensorimotor cortex in adult monkeys. *Exp. Brain Res., 128*, 149-159.

Logothetis, N. K., Pauls, J., Augath, M., Trinath, T., & Oeltermann, A. (2001). Neurophysiological investigation of the basis of the fMRI signal. *Nature, 412*, 150-157.

Magistretti, P. J., & Allaman, I. (2015). A cellular perspective on brain energy metabolism and functional imaging. *Neuron, 86*, 883-901.

Muir, R. B., & Lemon, R. N. (1983). Corticospinal neurons with a special role in precision grip. *Brain Res., 261*, 312-316.

Nili, H., Wingfield, C., Walther, A., Su, L., Marslen-Wilson, W., & Kriegeskorte, N. (2014). A toolbox for representational similarity analysis. *PLoS Comput. Biol., 10*, e1003553.

Poliakov, A. V., & Schieber, M. H. (1999). Limited functional grouping of neurons in the motor cortex hand area during individuated finger movements: A cluster analysis. *J. Neurophysiol., 82*, 3488-3505.

Pruszynski, J. A., Kurtzer, I., Nashed, J. Y., Omrani, M., Brouwer, B., & Scott, S. H. (2011). Primary motor cortex underlies multi-joint integration for fast feedback control. *Nature, 478*, 387-390.

Sasaki, S., Isa, T., Pettersson, L.-G., Alstermark, B., Naito, K., Yoshimura, K., . . . Ohki, Y. (2004). Dexterous finger movements in primate without monosynaptic corticomotoneuronal excitation. *J. Neurophysiol., 92*, 3142-3147.

Schieber, M. H. (1991). Individuated finger movements of rhesus monkeys: a means of quantifying the independence of the digits. *J. Neurophysiol., 65*, 1381-1391.

Schieber, M. H. (1990). How might the motor cortex individuate movements? *Trends Neurosci., 13*, 440-445.

Schieber, M. H., & Hibbard, L. S. (1993). How somatotopic is the motor cortex hand area? *Science, 261*, 489-492.

Schieber, M. H., & Poliakov, A. V. (1998). Partial inactivation of the primary motor cortex hand area: effects on individuated finger movements. *J. Neurosci., 18*, 9038-9054.

bioRxiv preprint doi: https://doi.org/10.1101/2020.03.17.996124; this version posted March 18, 2020. The copyright holder for this preprint (which was not certified by peer review) is the author/funder. All rights reserved. No reuse allowed without permission.

Schieber, M. H., & Rivlis, G. (2005). A spectrum from pure post-spike effects to synchrony effects in spike-triggered averages of electromyographic activity during skilled finger movements. *J. Neurophysiol., 94*, 3325-3341.

Schieber, M. H., & Rivlis, G. (2007). Partial reconstruction of muscle activity from a pruned network of diverse motor cortex neurons. *J. Neurophysiol., 97*, 70-82.

Tower, S. S. (1940). Pyramidal lesion in the monkey. *Brain, 63*, 36-90.

Valero-Cuevas, F. J., Zajac, F. E., & Burgar, C. G. (1998). Large index-fingertip forces are produced by subject-independent patterns of muscle excitation. *J. Biomech., 31*, 693-703.

Walther, A., Nili, H., Ejaz, N., Alink, A., Kriegeskorte, N., & Diedrichsen, J. (2016). Reliability of dissimilarity measures for multi-voxel pattern analysis. *Neuroimage, 137*, 188-200.

Wiestler, T., & Diedrichsen, J. (2013). Skill learning strengthens cortical representations of motor sequences. *eLife, 2*.

Wiestler, T., McGonigle, D. J., & Diedrichsen, J. (2011). Integration of sensory and motor representations of single fingers in the human cerebellum. *J. Neurophysiol., 105*, 3042-3053.

Xu, J., Ejaz, N., Hertler, B., Branscheidt, M., Widmer, M., Faria, A. V., . . . Diedrichsen, J. (2017). Separable systems for recovery of finger strength and control after stroke. *J. Neurophysiol., 118*, 1151-1163.

Young, N. A., Collins, C. E., & Kaas, J. H. (2013). Cell and neuron densities in the primary motor cortex of primates. *Front. Neural Circuits, 7*, 30.

Yousry, T. A., Schmid, U. D., Alkadhi, H., Schmidt, D., Peraud, A., Buettner, A., & Winkler, P. (1997). Localization of the motor hand area to a knob on the precentral gyrus. A new landmark. *Brain, 120 (Pt 1)*, 141-157.

Yu, B. M., Cunningham, J. P., Santhanam, G., Ryu, S. I., Shenoy, K. V., & Sahani, M. (2009). Gaussian-process factor analysis for low-dimensional single-trial analysis of neural population activity. *J. Neurophysiol., 102*, 614-635.

Yu, W. S., Duinen, H., & Gandevia, S. C. (2010). Limits to the control of the human thumb and fingers in flexion and extension. *J. Neurophysiol., 103*, 278-289.

Yu, Y., Herman, P., Rothman, D. L., Agarwal, D., & Hyder, F. (2018). Evaluating the gray and white matter energy budgets of human brain function. *Journal of Cerebral Blood Flow & Metabolism, 38*, 1339-1353.